Theses and Dissertations

2014

A Computational Model of Cell Spreading, Movement, and Alignment on Micro-Wavy Surfaces

Ezgi Pinar Yalcintas
Lehigh University

A COMPUTATIONAL MODEL OF CELL SPREADING, MOVEMENT, AND ALIGNMENT ON MICRO-WAVY SURFACES

by

Ezgi Pinar Yalcintas

A Thesis

Presented to the Graduate and Research Committee

of Lehigh University

in Candidacy for the Degree of

Master of Science

in

Mechanical Engineering

Lehigh University

May 2014

This thesis is accepted and approved in partial fulfillment of the requirements for the Master of Science.

_____
Date

_____
Professor Arkady Voloshin

_____
Professor Gary Harlow

TABLE OF CONTENTS

iv

LIST OF FIGURES

surface. Thus, IC Set1 is not applied to the slope position cases. (NR=non-rotated model, R=rotated model)

Figure 7: Total number of iterations within the simulation process until the cell model becomes spread on prescribed surfaces (the cell reaches half of its initial height). IC Set1 is not applied to the slope position cases. (NR=non-rotated model, R=rotated model)

Figure 8: Alignment angle definition

Figure 9: Alignment angle definition on ellipsoid

Figure 10: Ellipsoids fitted to coordinate data for the final spread configurations of the model that are initially placed at flat (A), trough (B), and peak (C) positions of wavy surface (NR-IC Set 1 case)

Figure 11: Ellipsoids fitted to coordinate data for the final spread configurations of the model that are initially placed at flat (A), trough (B), slope (C), and peak (D) positions of wavy surface (NR-IC Set 2 case)

Figure 12: Ellipsoids fitted to coordinate data for the final spread configurations of the model that are initially placed at flat (A), trough (B), and peak (C) positions of wavy surface (R-IC Set 1 case)

Figure 13: Ellipsoids fitted to coordinate data for the final spread configurations of the model that are initially placed at flat (A), trough (B), slope (C), and peak (D) positions of wavy surface (R-IC Set 2 case)

Figure 14: Alignment angles for different set of initial conditions and orientations for the model initially located at flat, trough, slope, and peak positions of the wavy surface (NR=non-rotated, R=rotated)

Figure 15: Scatter plot of the centroids, where red point represents the centroid of the undeformed (initial) model: isometric view (A), top view (XY plane) (B), and front view (XZ plane) (C) (F = flat, T=trough, P = peak, S = slope)

Figure 16: Spreading areas on the prescribed surface profiles for the final spread configurations of the model (NR=non-rotated, R=rotated)

LIST OF TABLES

ABSTRACT

Mechanical behavior of cells plays a crucial role in response to external stimuli and environment. It is very important to elucidate the mechanisms of cellular activities like spreading and alignment as it would shed light on further biological concepts.

A multi-scale computational approach is adopted by modeling the cytoskeleton of cell as a tensegrity structure. The model is based on the complementary force balance between the tension and compression elements, resembling the internal structure of cell cytoskeleton composed of microtubules and actin filaments. The effect of surface topology on strain energy of a spread cell is investigated by defining strain energy of the structure as the main criterion in the simulation process of the cell spreading.

Spreading as a way to decrease internal energy toward a minimum energy state is the main hypothesis that is investigated. The cell model is placed at different positions along the wavy surface and the spreading and alignment behavior is observed. The implementation of the model illustrates the effect of topological factors on spreading and alignment of the cell. The proposed computational model can be explanatory in terms of understanding mechanical characteristics of cells.

1

1. INTRODUCTION

Exposure to any physical environment that influences the cell's physical and internal balance leads to changes in its geometry and motion since a cell needs to maintain its structure and molecular self-assembly (Stamenovic and Ingber, 2009). These responses are basically due to mechanical loads or cell-generated forces that occur during the activities of cells in regulating cell functions like migration, differentiation, and growth (Chen et al., 1997). Mechanical signals that cells sense with surface receptors are transduced into chemical and biological response via the interconnected structure, namely the cytoskeleton that also serves as a stabilization mechanism of cell shape due to its filamentous network structure (Ingber, 1997).

The living cells exhibit mechanical and physical characteristics that enable them to respond to changes in their physical environment and internal structure. To better understand and analyze these complex structures, various mechanical models have been developed in recent years. Some of the mechanical cell models represent the cell as a continuum structure by assigning material characteristics where the intercellular functions and transmitting subcellular components are not modeled in detail. Liquid drop models, solid models, power-law structural damping models, and biphasic models can be categorized as continuum mechanical models (Lim et al., 2006). One of the developed liquid models is the Newtonian liquid drop model

(Yeung and Evans, 1989) in which the cytoplasm is modeled as a Newtonian viscous liquid and the cortex as a viscous fluid layer with constant static tension. Shear thinning liquid drop model (Tsai et al., 1993), and Maxwell liquid drop model (Dong et al., 1988) are further examples of liquid drop models that were developed to gain an insight in cell mechanics.

Another category of cell modeling includes solid models such as linear elastic solid model (Theret et al., 1988) and linear viscoelastic solid model (Schmid-Schonbein et al., 1981) that were first derived to ascertain the small-strain deformation characteristics of leukocytes. Power-law structural damping models (Alcaraz et al., 2003) deal with the dynamic characteristics of the cells whereas previously mentioned models are mostly obtained using transient conditions (Lim et al., 2006).

On the other hand, some models were derived using a micro-structural approach that deals with the underlying mechanics of cytoskeleton. These models are based on the idea that the mechanical behavior of a cell mainly depends on the filamentous structure, the cytoskeleton, by means of its components such as microtubules, microfilaments and intermediate filaments that are in the form of an integrated network (Wang et al., 2001). Wide range of cytoskeletal models have been developed using numerical and computational tools (Stamenovic and Ingber, 2002). One of the cytoskeletal models is the open-cell foam model in which the cross-linked network is considered as a porous solid matrix (Satcher and Dewey, 1996). Another model treats the cytoskeleton as a prestressed cable network in

order to predict the elastic properties and emerging forces by deforming the model mechanically (Coughlin and Stamenovic, 2003). A further mechanical model was proposed by Maurin et al. (2008), in which the form-finding structure of the cytoskeleton is investigated by using a granular structure representing the interconnected network of filaments in cytoskeleton. Also, a semi-flexible network approach is used by Roy and Qi (2008) with the aim of gaining an insight in deformation mechanics and elastic characteristics of the network model.   In addition to mechanical models of cytoskeleton, an architectural structure 'tensegrity' has been used for modeling the interconnected network of filaments since the existence of compression and tension members in the tensegrity structure represents the mechanical force balance and the sustainability in cytoskeleton (Coughlin and Stamenovic, 1998; Stamenovic et al., 1996; and Ingber, 2008). The tensegrity structure is used to explain cell motility and shape changes of the cell since it provides a comprehensive approach where the mechanical integrity is maintained and a self-equilibrium is obtained through the contribution of actin filaments that are under tension and microtubules that are under compression (Ingber, 2003; and Ingber, 2008). To gain a deeper understanding in the architectural structure of cytoskeleton on the basis of tensegrity concept several finite element models were developed to explain the non-linear structural behavior (McGarry and Prendergast, 2004), the mechanotransmission processes using mechanical perturbations (Wendling et al., 2002), or the viscoelastic contraction-

4

retraction of the pretensed network using a multi-modular approach of tensegrity (Luo et al., 2008).

From a computational point of view (Sander et al., 2009; and Cukierman et al., 2001) it can be concluded that the cell does not interact continuously with its surroundings, but actually forms attachments that are distributed in a non-affine and heterogeneous fashion. The tensegrity structure (Ingber, 2006) will be appropriate to model such behavior. Till now, the mechanism by which the mechanical forces applied at the macroscopic scale influence specific molecular activities remains unknown in most somatic organ systems. Tensegrity modeling allows to create a model of the cell and show how the cell's behavior depends on the surface topography. When a cell attaches to a particular surface, it changes its geometry, effectively as if external forces were applied to the cell membrane to force its deformation. Thus, mechanotransduction is not only the reaction of the cell to the external mechanical effects, but also the reaction of the cell to the change of the surface topography. Study of structure interactions within the cell will provide important insight for understanding and modeling related molecular mechanisms. In order to elucidate the spreading and alignment phenomenon of cell, an approach based on total strain energy of a cell is employed. A similar approach was also employed by Li et al. (2010) where they implemented the Monte Carlo method based on minimizing the strain energy of the tensegrity structure for their optimization problem. In present study, the effect of the surface geometry on the change in the strain energy of a spread cell is evaluated. The cytoskeleton of a cell

was modeled as a tensegrity structure and its strain energy was calculated based on the geometry of surface it is attached using Finite Element Analysis tools.

Besides computational and analytical models, various experimental techniques were also used to study the influence of surface pattern on cell adhesion and orientation, since cellular interaction with micro-structured surfaces is very important for various biomedical applications from tissue engineering to lab-on-chip devices. In recent years, significant efforts have been made to develop micro-textured polymeric materials for application in biomedical systems (Feinberg et al., 2008; and Su et al., 2007). Cell patterning techniques (Kawashima et al., 2010; and Huh et al., 2012), which provide the basis approach for manipulating cells, play an important role in understanding functions of both individual cells and the cell-cell interaction.

Motility of cell may be encouraged by various factors, like chemotaxis (response to a chemical gradient) (Zhelev et al., 2004), galvanotaxis (response to a potential gradient) (Curtze et al., 2004), or mechanotaxis (response to the underlying surface rigidity) (Lo et al., 2000). In this study, we aimed at developing a multi-scale computational model defining "sensor" elements that probe the surface continuously and decide on the direction of spreading. The multi-scale model is used to understand the mechanics of cell-curved surface interaction – topotaxis, and compare the obtained results with the observed effects of the various curved micro-patterns on initial seeding, spreading and alignment of cells. We employed an approach in which the total strain energy is used as the main criterion

for spreading and alignment. Our hypothesis is based on the idea that cell tries to spread and move in a way to decrease its internal elastic energy and stay at a possible minimum energy state. This approach is implemented here to investigate the spreading characteristics of a cell on different topologies.

2. COMPUTATIONAL MODEL AND METHODS

2.1 MODELING CELL SPREADING PROCESS

2.1.1 Model Description

In this study, a 30 member tensegrity structure is used to model the cytoskeleton of a living cell. There are 6 pre-compressed struts and 24 pre-tensed cables in the cytoskeletal model. The struts are analogous to microtubule members which carry compressional loads, and the cables correspond to the microfilament members that bear the tensional loads. Since tensegrity is an architectural structure that maintains its stability due to the compression and tension members, the model is generated accordingly; having the members that bare tensile and compressive forces with specified material properties. The schematic of the cytoskeletal model is presented in Figure 1A-B.

The model is in equilibrium, which corresponds to the stage that the complementary force balance is preserved within the cytoskeletal members resulting in a stabilized and equilibrated model. There are 12 nodes in the model

that interconnect the struts and cables, representing the possible cell-matrix adhesion sites, namely focal adhesions (FAs), which create a linkage to the extracellular matrix (ECM). The computational model allows the strut and cable lengths to increase or decrease. The nodes are allowed to move in 3-D, representing the spreading and active movement of the cell. The initial tensegrity model has a height of 8.7 µm and the distance between struts is 5 µm to mimic the size of Bovine Aortic Endothelial Cells (BAECs). Nodes that are at the same elevation with respect to the x-y plane generate horizontal planes (layers) (Figure 2). The distance between the top and bottom planes for the undeformed structure defines the initial height of the cell. ANSYS Mechanical APDL[1] is used as the finite element analysis tool in which the model is created and simulations are held. The wavy surface has a period of 20 µm and a height (peak-to-peak amplitude) of 6.6 µm, which is assigned as the topological characteristics of the seeding surface. Initial configurations of the cell model on flat, trough, peak and slope positions are displayed in Figure 3.

The displacements are calculated from eq. 1

$$[k]\{d\} = \{r\} \qquad\qquad (1)$$

where *[k]* is the element stiffness coefficient matrix, *{d}* is the element nodal displacement vector and *{r}* is the vector of element nodal loads.

---

[1] ANSYS, Inc., Canonsburg, PA, USA

The force balance within the tensegrity structure is preserved with the complementary force balance of tension and compression members. Length of struts and cables are subject to change in order to conform to a balanced structure. Denoting cross sectional area as A_i, elastic modulus as E_i, length as L_i, and axial force as F_i; the change in length, e_i, for the ith cable or strut is given as,

$$e_i = \frac{F_i L_i}{A_i E_i} \qquad (2)$$

the stiffness is given as the ratio of force to displacement, which is denoted by k,

$$k_i = \frac{F_i}{e_i} = \frac{A_i E_i}{L_i} \qquad (3)$$

The total energy is sum of the strain energy of microtubules and actin filaments. Hence, the total strain energy is calculated by the following equation,

$$U_T = \frac{1}{2} \int_V \{\sigma\}_m{}^T \{\varepsilon\}_m \, dV_m + \frac{1}{2} \int_V \{\sigma\}_a{}^T \{\varepsilon\}_a \, dV_a \qquad (4)$$

where U_T denotes the total energy, $\{\sigma\}_m$ and $\{\varepsilon\}_m$ denote the stress and strain components for the microtubules respectively, $\{\sigma\}_a$ and $\{\varepsilon\}_a$ are the stress and strain components for the actin filaments respectively as well. V stands for the volume of the elements.

2.1.2 Mechanical Properties of Cellular Components

Several experiments are conducted in the pursuit of deriving mechanical properties of the cytoskeletal components in the previous years. In order to implement the flexural rigidity properties of microtubules and microfilaments, the results of experiments held by Gittes et al. (1993) are employed in which the thermally driven fluctuations are analyzed and subsequent values are estimated. Also, all the struts and cables are assumed to be elastic. For Poisson's ratio (v) value, 0.3 is used for both microtubules and microfilaments. The cross-sectional area of microtubules are used as 190.0e-06 whereas the microfilaments are modelled with a cross-sectional area of 19.00e-06 (Gittes et al., 1993). Also, initial length of microtubules are 10.00 μm (Coughlin and Stamenovic, 1998) which are subject to change in each subsequent simulation. The mechanical properties of constitutive elements in the tensegrity structure are also provided in Table 1.

2.1.3 Prestress and Initial Constraints

Prestress is the key factor in maintaining cell shape. Prestress is present within cytoskeleton (CSK) and originates from the tensional forces that occur in the microfilaments (Stamenovic, 2012). These forces are channeled across the intermediate cytoskeletal filaments and balanced by the compression elements, microtubules, and traction forces that are present at focal adhesions (Stamenovic and Ingber, 2009). Also, in addition to the vital cellular functions like cell

10

migration, cell spreading, proliferation and mechanical signaling through interconnections, many other fundamental functions within the cell could also be dependent on the level of the contractile prestress in living cells. Prestress also plays an important role in determining cellular stiffness as shown in experiments conducted with the use of prestressed actin networks (Gardel et al., 2006). This was also suggested in the experiments where a cell-stretching system was used to investigate the relationship between cell stiffness (Pourati et al., 1998) and prestress (Rosenblatt et al., 2004).

One of the unique characteristics of tensegrity structures is that they consist of prestressed members which provide the ability to preserve equilibrium even if no external force is applied on the structure (Sultan et al., 2004). Hence, it is a suitable approach to embed the concept of tensegrity into CSK modeling in order to simulate cell spreading and movement. In this study, the prestress on the cytoskeletal members is preserved as the microfilament stiffness varies. Contractile prestress within the model is acquired by imposing the corresponding tension and compression forces onto the nodes.

Initial constraints (IC) were defined for some nodes to simulate focal adhesions and cell-surface interactions. Rest of the nodes, which are not constrained, serve as candidates of FAs since the cell spreading is a continuous process and may lead those nodes to come into contact with the substrate surface.

In order to model the cell adhesion on surface after seeding, bottom nodes that are in contact with the surface are anchored to the surface to represent the focal adhesion sites. Two different set of bottom constraints are employed in the simulations. In the first set of constraints, nodes 2 and 3 are constrained in translational degree of freedom in z-direction. This type of constraint allows them to slide along the x-y plane during spreading of the cell; however, node 1 is anchored to the surface such that it is constrained in all translational degrees of freedom. In the second set of constraints, only node 1 is anchored to the prescribed surface and constrained in all translational degrees of freedom.

In addition to different bottom constraints, two different initial configurations of the model are employed in the simulations. In the first one the bottom plane of the model is horizontal and parallel to the flat surface, and three bottom nodes are at the same elevation. For the second case, the model is initially rotated ~12 degrees in x-direction.

2.1.4   Simulation Method and Modeling

Active adhesion and focal adhesion modeling can serve as an effective method in cell spreading on the ECM since this approach describes not only the passive formation of adhesive bonds by cell attachment process, but also the cell spreading. Hence, the prescribed model includes an important element capable to describe the sensing of the surface that cell is located upon. Sensing elements are introduced in

FE model that are able to randomly probe the surface close to the cell. The probing is modeled as an active element (node) capable to change its location and thus changing the cell's shape. The "sensors" moves to touch the surface, hence, the strain energy of the cell changes which is computed at each step. This information is used to decide on the probable movement of the cell toward and along the surface. In the proposed model, the cell randomly extends nodes and evaluates associated change in strain energy. This information will allow the cell to select the preferable direction of motion. The procedure will repeat such steps until the cell spreads on the surface. Due to the randomness in the extension of the "sensor", it is expected that this model is able to simulate the distribution of cells on the curved surface in a realistic manner.

The effects of gravity and magnetic field are neglected in the simulations. The approach and procedure of the simulation process are described as follows. In each iteration step, one of the nodes that is not constrained in translational degree of freedom is given an incremental displacement in z direction. As a result of this motion, strut and cable lengths and positions may change in accordance with the assigned material properties. Node locations alter within the constraints of the tensegrity structure. At the end of the load step, the total strain energy is calculated and stored in the database for further processing. The strain energy of the cytoskeleton is obtained by strain energy summation of all elements: struts and tension cables. After obtaining and storing the strain energy, the simulation returns back to the initial configuration step that it originates and all nodes relocate to their

initial positions. Hence, the initial state is obtained again. This time, another node that is not constrained is given an incremental displacement, and previously explained steps are repeated.

The simulation is repeated until all the nodes (except the constrained ones) are given an incremental displacement, and the resultant total strain energy values are stored for each generated configuration. Once the explained steps are executed within the algorithm, the decision making phase becomes effective. At this stage, a comparison is made between the total strain energy values. The configuration that has the lowest total strain energy from all configurations is selected. Hence, the corresponding node that resulted in a lower energy is chosen as the "sensor" node and given the incremental displacement. The application of this incremental displacement leads the cell to change its shape. The updated model and new locations of nodes are stored to be used as the new initial state of the cell in the consecutive iteration steps of the simulation. As a next step, which can be considered as a decision step, to check if the "sensor" node reaches the surface or if any other node makes a contact with the surface, the distance of each node with respect to the surface that the cell resides on is calculated and stored. These obtained values are then used to check whether the locations of nodes (with respect to the surface) are within the prescribed threshold value. If any node appears to be within the threshold value, then this node is constrained in z direction, but free to slide on x and y directions which mimics the focal adhesion site formed on the surface, binding the cell to ECM.

In the second phase of the decision step, the algorithm for the termination criterion is executed to check whether the height of cytoskeletal model reaches the half of its initial height after spreading on the prescribed topology. The specific height that is used as the termination criterion is based on the nucleocytoplasmic volume ratio ($R_{N/C}$) of BAECs. Experimental results investigating the affect of cellular dimension on nucleocytoplasmic volume ratio indicate that $R_{N/C}$ of endothelial cells is ~0.23 (Swanson et al., 1991). In order to preserve the volume of the rigid nucleus and to account for the spreading of the cell, half of the initial height of the cell is used as the final spread height. If the model reaches the desired height after spreading, then the iterations stop and simulation ends. If not, resultant motion that takes place due to the sensor node is taken into consideration and is used as the updated model. Modified state of the structure and new locations for each node are stored to be used as the new initial state of the cell and appropriate numerical implementation and enhancements are applied at the beginning of the consecutive iteration step. This iteration procedure is executed until the desired height of the cell is attained. Explanation of the steps in the simulation procedure is provided as a flow chart in Figure 4.

3. SIMULATION OF CELL SPREADING ON VARIOUS POSITIONS OF WAVY TOPOLOGY

To assess the tendency of the cell when spreading on different positions of the wavy surface and to understand the relationship between cell spreading and the change of elastic strain energy during spreading process, the cytoskeletal model was placed on different positions of the wavy surface.

Simulations are performed on flat, trough, peak and slope positions of the wavy profile to observe the interaction of an individual cell with specific topology and to test if the model attaches and spreads on the prescribed surface in a similar manner as experimental results indicate (Chen et al., 1998). The goal in each step of simulations is to obtain a configuration that leads to a lower strain energy state. This goal is pursued by deforming the model by giving incremental displacements to the nodes in order to find a sensor node by comparing the resulting strain energies for the trial configurations. Whichever node among the candidates favors the decrease in the system energy is chosen as the sensor and is imposed to the incremental motion.

To observe the effect of initial constraints on spreading kinetics, two different set of bottom constraints are imposed on the cytoskeletal model. Those constraints mimic the focal adhesion sites that are formed right after cell seeding. In the first set (initial constraint set 1), node 1 is pinned to the prescribed surface and

constrained in all translational degrees of freedom, which are x, y and z-directions. Nodes 2 and 3 are constrained only in z-direction, which gives them the ability to slide on x-y plane and simulate the spreading process. In the second set of constraints (initial constraint set 2), only node 1 is anchored to the prescribed surfaces and constraint in all translational degrees of freedom. For the slope position, only node 2 is anchored to the surface instead of node 1, hence it is also categorized as initial constraint set 2 since only one node is constrained in all directions. Simulations for the slope position are only handled with one set of initial constraints since it would not be realistic or possible to create more than one constraint on the slope due to the cell's initial position with respect to surface. Also, two different initial configurations of the model are employed in the simulations. In the first case, the bottom plane of the model is horizontal (non-rotated). Second one is where the model is rotated 12 degrees around x-axis. This is done to evaluate the effect of the cell's initial position on the resultant energy.

Spreading of the model on the flat surface for different cases of initial constraints and configurations did not show significant differences in terms of final shape. For each case of simulations, the cell models after spreading showed similarity by means of final shape and alignment. The final shape of non-rotated model on flat surface with second set of initial constraints applied can be seen in Figure 5A. Most of the nodes became the focal adhesion sites by making contact with the surface. As the spreading area increases, the shape tends to become conical, due to the sensor node movement. The decision criterion at each step of

iterations leads to the selection of a sensor node among other candidates. This criterion is based on selecting a node whose motion results in lower total strain energy when compared to the resultant energy of other candidates' movement.

When the final configuration for the trough position case is considered (Figure 5B), it should be noted that the model tried to spread within the troughs of the surface such that it fills the concave profile instead of spreading upwards. This type of behavior is observed in all four cases. However, when the final configurations for the peak position cases are considered (Figure 5C), the tendency of the cell to spread downward becomes prominent.

The results of simulations obtained by placing the cell initially on peak and trough positions indicate that the spreading of the cell that satisfies the criterion of obtaining a lower elastic energy is toward the lower part of the wavy profile. This can be interpreted as the proneness of the cell to fill the troughs of the wavy surface instead of staying at the crests. In Figure 5C, it can clearly be seen that the cell tended to spread toward the trough, whereas in Figure 5B, the cell stayed at the trough and spread along the direction of the wavy pattern.

The result of the slope position simulation indicates the tendency of the cell to spread downward to fill the trough instead of staying on the inclined part of the surface or spreading upward through the crest (Figure 5D). The final configuration of the cell is similar to the final resultant shape obtained by placing the cell model initially on the trough position of the surface. The cell spread on the surface and

tried to fill in the space that it sits on by attaching the sensor nodes to the surface, expanding in a way to increase its contact surface area. Hence, it can be concluded that the effective mechanism in decision making process can be the procedure of choosing a direction of spreading that leads to a lower energy level by moving the appropriate node that obeys the energy criterion and attains a level of spreading at a minimum number of incremental movements (Figure 7). Not only the cells on the wavy surface attach to the troughs of the waves, but they also align along the wave direction, which can explain the behavior of the cell to expand more on troughs of surfaces, resulting in a larger spreading area on contact surface.

The simulations on flat, trough, slope and peak positions used the same dimensional characteristics as the ones used in the experiments. The procedure of the simulation process is the same for flat, trough, and peak positions. The incremental movements of nodes take place, which are followed by decision making step. The only difference between the algorithm for slope position and other cases is that each iteration step is done by dividing it into two steps. In the first, one of the nodes that is not constrained in translational degrees of freedom is given an incremental displacement in –z and –x directions, to simulate the downward spreading of the cell through the trough of the wavy profile. In the second part of the iteration, the same node is given an incremental displacement in +z and +x directions this time, to simulate the upward spreading of the cell through the crest of the wavy profile. In each iteration step the decision criterion becomes effective to decide on the direction of motion for the node which would result in a

19

lower energy level than the reverse motion. At the next step, another node that is not constrained in translational degrees of freedom is given an incremental displacement, and previously explained steps are repeated. The simulation is repeated until all the nodes (except the constrained ones) are given the upward and downward incremental displacements, and the resultant total strain energy values are stored for each generated configuration. Then, a comparison is made between the total strain energy values. The configuration that has the lowest total strain energy is selected. The use of slope position on surface profile leads us to see what type of behavior is illustrated by the cell when seeded onto a curved surface. This observation serves as a guide in understanding the spreading kinetics and show whether the cell prefers to move toward the crest or trough.

4. EFFECTS OF CELL SPREADING ON ELASTIC ENERGY

The total resultant strain energy values for the spread configurations are obtained and shown in Figure 6A for the initial constraint set 1 with rotated and non-rotated model cases. The peak position leads to a higher energy value in both cases whereas the flat profile has the lowest final energy value for the non-rotated model. When the rotated model case is considered it is observed that the model initially placed on the trough position has a lower energy than the model placed on flat surface. For non-rotated and rotated cases, the final energy values for peak position does not show a significant difference, which means that the initial

position of the model does not affect the overall motion of cell in terms of energy. Hence, the model shows a similar behavior no matter how it is oriented at the initial seeding, which shows the independence of motion from initial orientation. Same conclusion can be made for the model initially placed on trough and slope positions of the surface. The resultant strain energy values appear to be comparable respectively, which also highlights the fact that placing the model on the surface with a different orientation by rotating the model does not affect the overall pattern of motion when the cell is seeded on peak, slope or trough positions. For the flat case, however, the difference of energy values is significant for the two set of initial orientations. This may be due to the fact that direction of motion is random on the flat surface. Since there is not a topological difference on the surface, there may not be a factor that triggers the cell to move at a preferable direction. Hence, the direction of motion is not decided upon analyzing topological differences, which may result in a random motion. The motion and energy levels of cell on flat surface may not be correlated to initial conditions since the simulations on flat surface can be considered as random. Resultant energy values obtained by imposing the initial constraint set 2 to the cell model (Figure 6B) also show that the energy level is the lowest for the rotated model that is initially placed on the trough position. In addition, energy level is highest for the peak positions similar to the observed results for the case where initial constraint set 1 is applied (Figure 6A). In agreement with the results that show the proneness of the cell to fill the troughs of the wavy surface (Figure 5B-C-D), the resultant strain energy values may also

21

show the tendency of the cell to spread downwards instead of staying at crests when the resultant energy values for trough and peak positions are considered.

On the basis of the minimum strain energy it can be stated that the spreading patterns and energy levels are independent from the cell initial orientation or the node restrictions of the model initially placed on the trough, peak, and slope positions of the surface (Figure 5B-C-D). The resultant energy levels do not show significant difference for non-rotated or rotated models when the cell is on trough, slope or at the peak. For the flat case, however, final energy levels show difference for the non-rotated and rotated initial configurations. The randomness in spreading on flat surface may be the main reason for such a result in energy levels. In terms of computational perspective, since the topology of a flat surface does not have geometrical variations as in a wavy surface, the model may not need to select a specific direction of spreading. As a result, the differences in the resultant energy levels may be due to the random taxis of the cell observed during spreading. Hence, it can be concluded that initial orientation of the model may not give comparable or gaugeable results on flat surface in terms of preferred direction of spreading. On the other hand, resultant energy levels for the cell that is placed on trough, slope, and peak show comparable and consistent results respectively. This means that the model shows the same behavior whether it is initially rotated or not. Hence, the initial orientation does not affect the overall spreading of the model when it is on peak, slope or trough. The resultant energy is highest for all cases of the model placed on peak, while the energy levels at the trough and slope positions are lower

than the peak position energy values in all cases (Figure 6A-B). In conformance with the results shown in Figure 5, the resultant strain energy values for the peak, slope and trough positions show the proneness of the cell to spread downwards and fill the troughs of the wavy surface. This might be due to the fact that the energy level is lower when the cell spreads downwards and fills in the troughs. Crests might not be the preferred locations to stay on or move through when seeded on the surface since the model tends to move in a way that the energy levels decrease or stay low, which might be satisfied by spreading downwards towards the troughs.

Total number of iterations until the model reaches the desired height by spreading on the surface indicates that the simulation takes more time for the peak position cases and it takes more steps to reach the desired level of spreading (Figure 7). However, the simulations end at a shorter time for the trough and flat positions in all the cases.

The total numbers of iterations for each set of simulations can be explanatory in terms of optimum cell motion. Combined with the results of strain energy values (Figure 6A-B), iteration numbers may indicate that the cell may prefer to spread in such a way that the final configuration with lower energy is achieved at the shortest possible time, or with less movement. This might be the underlying mechanism of cell spreading and the decision making process during cell spreading and alignment.

The nodes that are at the same elevation form planes (layers) parallel to each other. At first sight, one can hypothesize that the nodes which are closer to the surface should be selected as sensor nodes and move downwards through the surface in the iterative steps of spreading since it would be easier to spread from bottom to top. This type of motion would be more feasible for the lower nodes since they can sense the underlying surface easier than the nodes located at higher elevations. As expected, at the first steps of iterations, the nodes that are at lower locations (nodes 4, 5, 6) are chosen as sensors since they are closer to the surface and can sense the ground better than the nodes located at higher elevations. After some degree of spreading is attained and new focal adhesion sites are formed, nodes that locate at higher positions compared to the bottom nodes start to move as well since they are now the candidates as sensors and can easily sense the ground. This process continues until the cell spreads on the surface and reaches half of its initial height. The spreading proceeds as follows: the nodes that form the second layer (nodes 4, 5, 6) move at the initial steps of iterations, than the nodes forming the third (nodes 7, 8, 9) and fourth (nodes 10, 11, 12) layers start to move in the following iteration steps. After that, the selection of sensor nodes, based on the energy criterion within the algorithm, becomes independent from the layers since the cell is spread some amount and the locations of the nodes cannot be categorized as done previously. Hence, the nodes that are now closer to the surface in the new configurations serve as candidates for sensors obeying the criterion based on lowering the total strain energy.

5. CELL ALIGNMENT AND ELONGATION

The orientation and alignment characteristics of cells have been studied by means of reaction to external stimuli (Noria et al., 2004). Topological effects on cell alignment have also been shown by Lam et al., (2008) by observing the reorientation and alignment of myoblast cells on reversible waves. In present study, the effect of alignment angle is investigated by observing simulation of the cells spreading on the wavy pattern after cell seeding and measuring the alignment angle.

The cell alignment angle is defined as the angle between the long axis of the cell and the direction of the wavy pattern (Figure 8 and Figure 9). Alignment angles of spread models are obtained for each set of initial constraints and configurations for the model initially located on the flat, trough, peak, and slope positions of the surface. An ellipsoid was fitted using the coordinate data of nodes at the final spread configuration of the model. Plots for the ellipsoids that represent the non-rotated initial condition set 1, non-rotated initial condition set 2, rotated initial condition set 1, and rotated initial condition set 2 cases are demonstrated in Figures 10, 11, 12, and 13 respectively. Also, the alignment angles for the models at flat, trough, peak and slope positions are provided in Figure 14. As it can be seen, the alignment angles for the peak position are larger than angle values for the flat, trough and slope positions for all the different sets of initial conditions, and range

between 40° and 42° (Figure 14). For the slope position, the alignment angle values are between 31° and 32°, whereas for trough position the alignment angles take values that range between 15° and 19°. This result compares well with the aforementioned comments, emphasizing the tendency of the cells to move towards the trough positions instead of staying at crests. Alignment angles are larger for the peak and slope positions which indicate that cells reorient themselves to move in a way to fill in the troughs. For the flat position, however, cell alignment angles are small; which can be due to the uniform distribution of nodes on the flat surface, which manifests random orientation of cells on the substrate. Hence, alignment angle results for the flat surface may also reveal the randomness of motion on flat surface, in agreement with results concluded by interpreting the elastic energy results.

In order to understand the movement of cells on wavy surface, the centroids of the initial configuration of cell and spread cells are found. Figure 15 shows the positions of centroids. As it can be seen in the figure, the centroid positions demonstrate the overall movement of cells on the wavy and flat surfaces. The centroid positions on XY plane provide complementary results for the alignment and elongation behavior of the cells (Figure 15B). Also, the degree of spreading in terms of final height is observed in Figure 15C, which shows the height of centroids with respect to the underlying surface.

6. EFFECTS ON SPREADING AREA

The model shows different amount of spreading on different surface topologies. The surface area of the cell in contact with the surface at the final stage of spreading on concave profile is larger in all cases, whereas the spreading area is smaller on the convex profile (Figure 16). This result demonstrates the tendency of the cell to fill in the troughs of wavy surface, similar to the aforementioned results. Instead of heading towards the sides and trying to crawl upwards, the model prefers to expand and increase its surface area as a result of the movement of sensor nodes that are in contact with the surface, mimicking the FAs.

7. CONCLUSIONS

The aim of this investigation is to study the mechanics of cell-curved surface interaction through a computational model of cell cytoskeleton based on the tensegrity structure. Cells are placed on different positions of the wavy surface topology to investigate the possible active mechanisms that control the spreading and alignment of the cell and the preferred locations on wavy surfaces that the cell is most likely to bind on and spread. The prominence of changes in strain energy during spreading phenomenon is observed by controlling the decision making process of sensor node selection. The principal findings are as follows.

The simulations obtained by placing the cell initially on peak and slope positions show that the criterion of obtaining a lower elastic energy during spreading is satisfied when the cell prefers to move toward the lower part of the wavy profile. When the cell is initially positioned at the trough position of the wavy surface, it is seen that the cell spread on the surface and tried to fill in the space by attaching the sensor nodes to the underlying surface. These results indicate the tendency of the cell to fill the troughs of the wavy surface instead of staying at the crests or crawling upwards.

In terms of elastic energy, non-rotated and rotated cases do not show a significant difference in final elastic energy values for the cells located at peak, slope, and trough positions; which means that the movement behavior of the cell is

independent of the initial orientation of the model and starting configuration does not affect the motion energy wise.

For the flat case, however, the energy values show significant difference for the cases having different initial orientations. In contrast to a wavy profile, a flat surface does not have topological variances; hence, there is not a topological cue that influences the cell decision on the direction of motion. As a result, the motion pattern is independent of the initial orientation of the cell, which may result in a random motion of the cell on flat surface.

Total iteration numbers until the model reaches the desired final height reveal an important result when interpreted together with the aforementioned results. The effective mechanism in decision making procedure can be in a way to choose a motion pattern and direction by relocating the sensor nodes, which results in a lower elastic energy at minimum number of incremental movements. This result is important since it can explain the basic behavior of cell in a simplified context which can be the backbone criteria of further complex and detailed cell models.

The alignment of cells is also observed. Alignment angles are larger for the models located on peak position, which are followed by the decreasing values of angles for the slope, trough and flat positions respectively. Alignment angles are larger for the peak and slope positions showing the proneness of the cells to reorient themselves through the troughs. However, when the flat position is considered, it is seen that the alignment angles are small; which can result due to

the uniform distribution of nodes on the flat surface. This result also demonstrates the random motion of cells on flat surface.

The sensor nodes can be considered as the lamellipodium within the cell, a branched actin filament network, which triggers the motion of the cell by extending in the chosen direction of motion. Experiments conducted by Verkhovsky et al. (2003) show that the growth and density changes of actin filaments which exist within the lamellipodium has a distinct effect on orientation and motility. Hence, implementing a procedure that actively controls the direction of motion can be considered as mimicking the role of lamellipodium and may be readily explained within the frame of spreading behavior. As a final remark, by analyzing the cell response to wavy surfaces by making use of the computational observations, it can be concluded that cells response to topological cues.

8. LIST OF REFERENCES

Alcaraz, J., Buscemi, L., Grabulosa, M., Trepat, X., Fabry, B., Farré, R., & Navajas, D. (2003). Microrheology of human lung epithelial cells measured by atomic force microscopy. *Biophysical journal*, *84*(3), 2071-2079.

Chen, C. S., Mrksich, M., Huang, S., Whitesides, G. M., & Ingber, D. E. (1997). Geometric control of cell life and death. *Science*, *276*(5317), 1425-1428.

Chen, C. S., Mrksich, M., Huang, S., Whitesides, G. M., & Ingber, D. E. (1998). Micropatterned surfaces for control of cell shape, position, and function. *Biotechnology Progress*, *14*(3), 356-363.

Coughlin, M. F., & Stamenovic, D. (1998). A tensegrity model of the cytoskeleton in spread and round cells. *Journal of biomechanical engineering*, *120*(6), 770-777.

Coughlin, M. F., & Stamenović, D. (2003). A prestressed cable network model of the adherent cell cytoskeleton. *Biophysical journal*, *84*(2), 1328-1336.

Cukierman, E., Pankov, R., Stevens, D. R., & Yamada, K. M. (2001). Taking cell-matrix adhesions to the third dimension. *Science*, *294*(5547), 1708-1712.

Curtze, S., Dembo, M., Miron, M., & Jones, D. B. (2004). Dynamic changes in traction forces with DC electric field in osteoblast-like cells. *Journal of cell science*, *117*(13), 2721-2729.

Dong, C., Sung, K. L. P., Schmid-Schönbein, G. W., Chien, S., & Skalak, R. (1988). Passive deformation analysis of human leukocytes. *Journal of biomechanical engineering*, *110*(1), 27-36.

Feinberg, A. W., Wilkerson, W. R., Seegert, C. A., Gibson, A. L., Hoipkemeier‐Wilson, L., & Brennan, A. B. (2008). Systematic variation of microtopography, surface chemistry and elastic modulus and the state dependent effect on endothelial cell alignment. *Journal of Biomedical Materials Research Part A*, *86*(2), 522-534.

Gardel, M. L., Nakamura, F., Hartwig, J. H., Crocker, J. C., Stossel, T. P., & Weitz, D. A. (2006). Prestressed F-actin networks cross-linked by hinged filamins

31

replicate mechanical properties of cells. *Proceedings of the National Academy of Sciences of the United States of America*, *103*(6), 1762-1767.

Gittes, F., Mickey, B., Nettleton, J., & Howard, J. (1993). Flexural rigidity of microtubules and actin filaments measured from thermal fluctuations in shape. *The Journal of cell biology*, *120*(4), 923-934.

Huh, D., Torisawa, Y. S., Hamilton, G. A., Kim, H. J., & Ingber, D. E. (2012). Microengineered physiological biomimicry: organs-on-chips. *Lab on a chip*, *12*(12), 2156-2164.

Ingber, D. E. (1997). Tensegrity: the architectural basis of cellular mechanotransduction. *Annual review of physiology*, *59*(1), 575-599.

Ingber, D. E. (2003). Tensegrity I. Cell structure and hierarchical systems biology. *Journal of Cell Science*, *116*(7), 1157-1173.

Ingber, D. E. (2006). Cellular mechanotransduction: putting all the pieces together again. *The FASEB journal*, *20*(7), 811-827.

Ingber, D. E. (2008). Tensegrity and mechanotransduction. *Journal of bodywork and movement therapies*, *12*(3), 198-200.

Kawashima, T., Kimura, T., Shibata, T., Kishida, A., Mineta, T., & Makino, E. (2010). Feasibility study on cellular network analysis with patterned cell culture microdevice. *Microelectronic Engineering*, *87*(5), 704-707.

Lam, M. T., Clem, W. C., & Takayama, S. (2008). Reversible on-demand cell alignment using reconfigurable microtopography. *Biomaterials*, *29*(11), 1705-1712.

Li, Y., Feng, X. Q., Cao, Y. P., & Gao, H. (2010). A Monte Carlo form-finding method for large scale regular and irregular tensegrity structures. *International Journal of Solids and Structures*, *47*(14), 1888-1898.

Lim, C. T., Zhou, E. H., & Quek, S. T. (2006). Mechanical models for living cells—a review. *Journal of biomechanics*, *39*(2), 195-216.

Lo, C. M., Wang, H. B., Dembo, M., & Wang, Y. L. (2000). Cell movement is guided by the rigidity of the substrate. *Biophysical journal*, *79*(1), 144-152.

Luo, Y., Xu, X., Lele, T., Kumar, S., & Ingber, D. E. (2008). A multi-modular tensegrity model of an actin stress fiber. *Journal of biomechanics*, *41*(11), 2379-2387.

Maurin, B., Cañadas, P., Baudriller, H., Montcourrier, P., & Bettache, N. (2008). Mechanical model of cytoskeleton structuration during cell adhesion and spreading. *Journal of biomechanics*, *41*(9), 2036-2041.

McGarry, J. G., & Prendergast, P. J. (2004). A three-dimensional finite element model of an adherent eukaryotic cell. *Eur Cell Mater*, *7*, 27-33.

Noria, S., Xu, F., McCue, S., Jones, M., Gotlieb, A. I., & Langille, B. L. (2004). Assembly and reorientation of stress fibers drives morphological changes to endothelial cells exposed to shear stress. *The American journal of pathology*, *164*(4), 1211-1223.

Pourati, J., Maniotis, A., Spiegel, D., Schaffer, J. L., Butler, J. P., Fredberg, J. J., ... & Wang, N. (1998). Is cytoskeletal tension a major determinant of cell deformability in adherent endothelial cells?. *American Journal of Physiology-Cell Physiology*, *274*(5), C1283-C1289.

Rosenblatt, N., Hu, S., Chen, J., Wang, N., & Stamenović, D. (2004). Distending stress of the cytoskeleton is a key determinant of cell rheological behavior. *Biochemical and biophysical research communications*, *321*(3), 617-622.

Roy, S., & Qi, H. J. (2008). Micromechanical model for elasticity of the cell cytoskeleton. *Physical Review E*, *77*(6), 061916.

Sander, E. A., Stylianopoulos, T., Tranquillo, R. T., & Barocas, V. H. (2009). Image-based multiscale modeling predicts tissue-level and network-level fiber reorganization in stretched cell-compacted collagen gels. *Proceedings of the National Academy of Sciences*, *106*(42), 17675-17680.

Satcher Jr, R. L., & Dewey Jr, C. F. (1996). Theoretical estimates of mechanical properties of the endothelial cell cytoskeleton. *Biophysical journal*, *71*(1), 109-118.

Schmid-Schonbein, G. W., Sung, K. L., Tözeren, H., Skalak, R., & Chien, S. (1981). Passive mechanical properties of human leukocytes. *Biophysical Journal*, *36*(1), 243-256.

Stamenović, D., Fredberg, J. J., Wang, N., Butler, J. P., & Ingber, D. E. (1996). A microstructural approach to cytoskeletal mechanics based on tensegrity. *Journal of Theoretical Biology*, *181*(2), 125-136.

Stamenović, D., & Ingber, D. E. (2002). Models of cytoskeletal mechanics of adherent cells. *Biomechanics and modeling in mechanobiology*, *1*(1), 95-108.

Stamenović, D., & Ingber, D. E. (2009). Tensegrity-guided self assembly: from molecules to living cells. *Soft Matter*, *5*(6), 1137-1145.

Stamenović, D. (2012). Cytoskeletal prestress as a determinant of deformability and rheology of adherent cells. In *Cell and Tissue Engineering* (pp. 92-118). Springer Berlin Heidelberg.

Su, W. T., Liao, Y. F., & Chu, I. (2007). Observation of fibroblast motility on a micro-grooved hydrophobic elastomer substrate with different geometric characteristics. *Micron*, *38*(3), 278-285.

Sultan, C., Stamenović, D., & Ingber, D. E. (2004). A computational tensegrity model predicts dynamic rheological behaviors in living cells. *Annals of biomedical engineering*, *32*(4), 520-530.

Swanson, J. A., Lee, M., & Knapp, P. E. (1991). Cellular dimensions affecting the nucleocytoplasmic volume ratio. *The Journal of cell biology*, *115*(4), 941-948.

Theret, D. P., Nerem, R. M., Wheeler, L. T., Levesque, M. J., & Sato, M. (1988). The application of a homogeneous half-space model in the analysis of endothelial cell micropipette measurements. *Journal of biomechanical engineering*, *110*(3), 190-199.

Tsai, M. A., Frank, R. S., & Waugh, R. E. (1993). Passive mechanical behavior of human neutrophils: power-law fluid. *Biophysical journal*, *65*(5), 2078-2088.

Verkhovsky, A. B., Chaga, O. Y., Schaub, S., Svitkina, T. M., Meister, J. J., & Borisy, G. G. (2003). Orientational order of the lamellipodial actin network as demonstrated in living motile cells. *Molecular biology of the cell*, *14*(11), 4667-4675.

Wang, N., Naruse, K., Stamenović, D., Fredberg, J. J., Mijailovich, S. M., Tolić-Nørrelykke, I. M., ... & Ingber, D. E. (2001). Mechanical behavior in living cells

consistent with the tensegrity model. *Proceedings of the National Academy of Sciences*, *98*(14), 7765-7770.

Wendling, S., Cañadas, P., Oddou, C., & Meunier, A. (2002). Interrelations between elastic energy and strain in a tensegrity model: contribution to the analysis of the mechanical response in living cells. *Computer Methods in Biomechanics & Biomedical Engineering*, *5*(1), 1-6.

Yeung, A., & Evans, E. (1989). Cortical shell-liquid core model for passive flow of liquid-like spherical cells into micropipets. *Biophysical journal*, *56*(1), 139-149.

Zhelev, D. V., Alteraifi, A. M., & Chodniewicz, D. (2004). Controlled pseudopod extension of human neutrophils stimulated with different chemoattractants. *Biophysical journal*, *87*(1), 688-695.

APPENDIX

Additional figures are provided in this appendix. The information in these figures provides complementary results for the research findings provided in the main text. Figures A1, A2, A3, and A4 represent the final spread configurations of the cytoskeletal model at the end of simulations for non-rotated case initial constraint set 1 and set 2, and rotated case initial constraint set 1 and set 2 for flat, trough, slope, and peak positions of the wavy profile, respectively. All different cases of initial configurations and orientations are provided in these figures providing complementary and extended information to Figure 5 given in the main text.
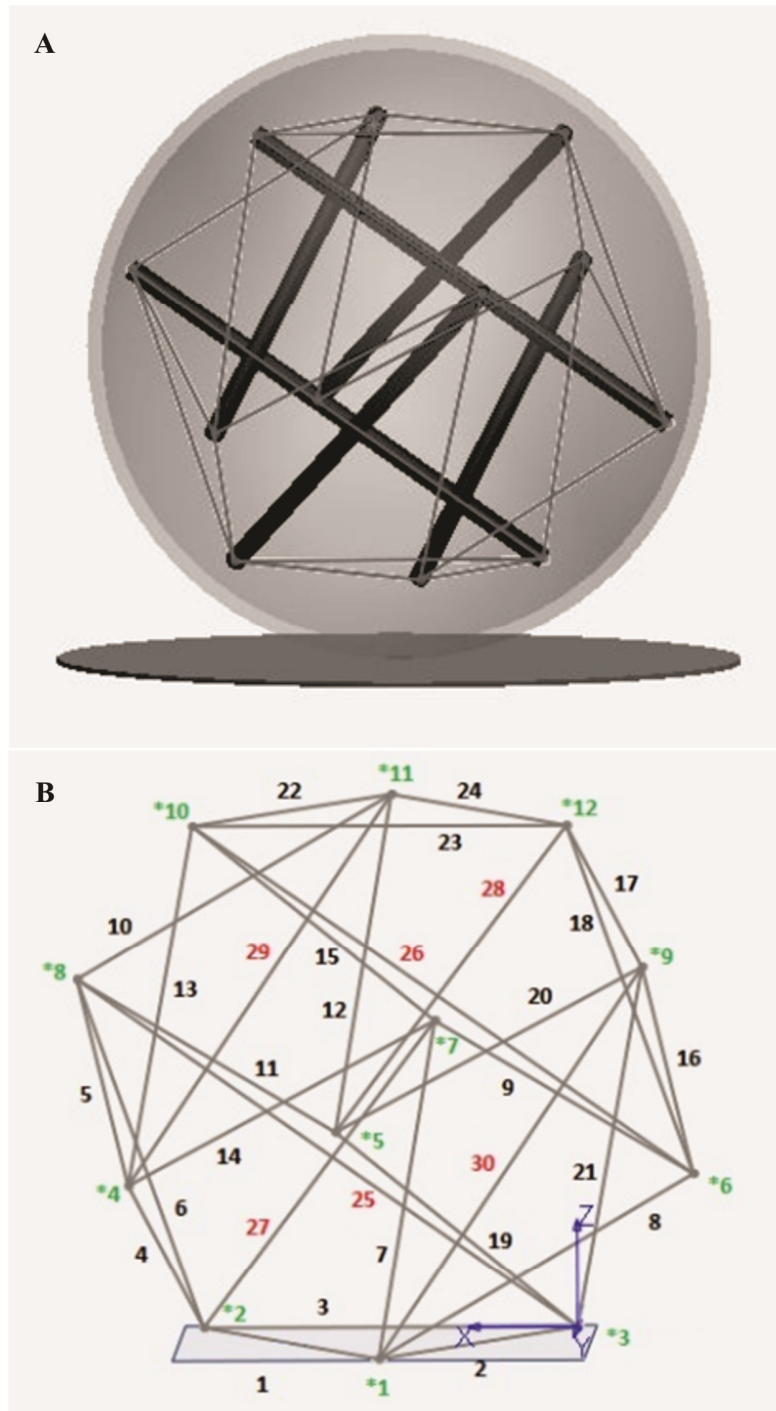
Figure 1: Cytoskeletal tensegrity model (A). Black colored numbering represents the microfilaments (cables), red colored numbering represents the microtubules (struts), and the node numbers are shown as green (B)
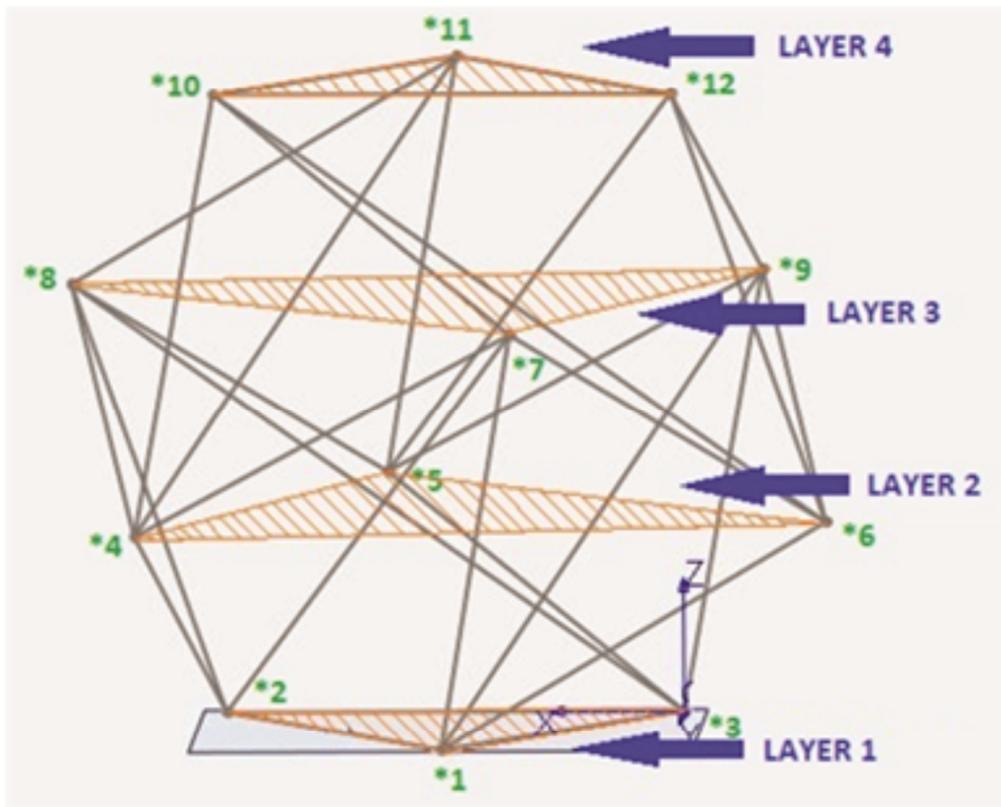
Figure 2: Horizontal planes (layers) formed by the nodes that are at the same elevation with respect to the x-y plane
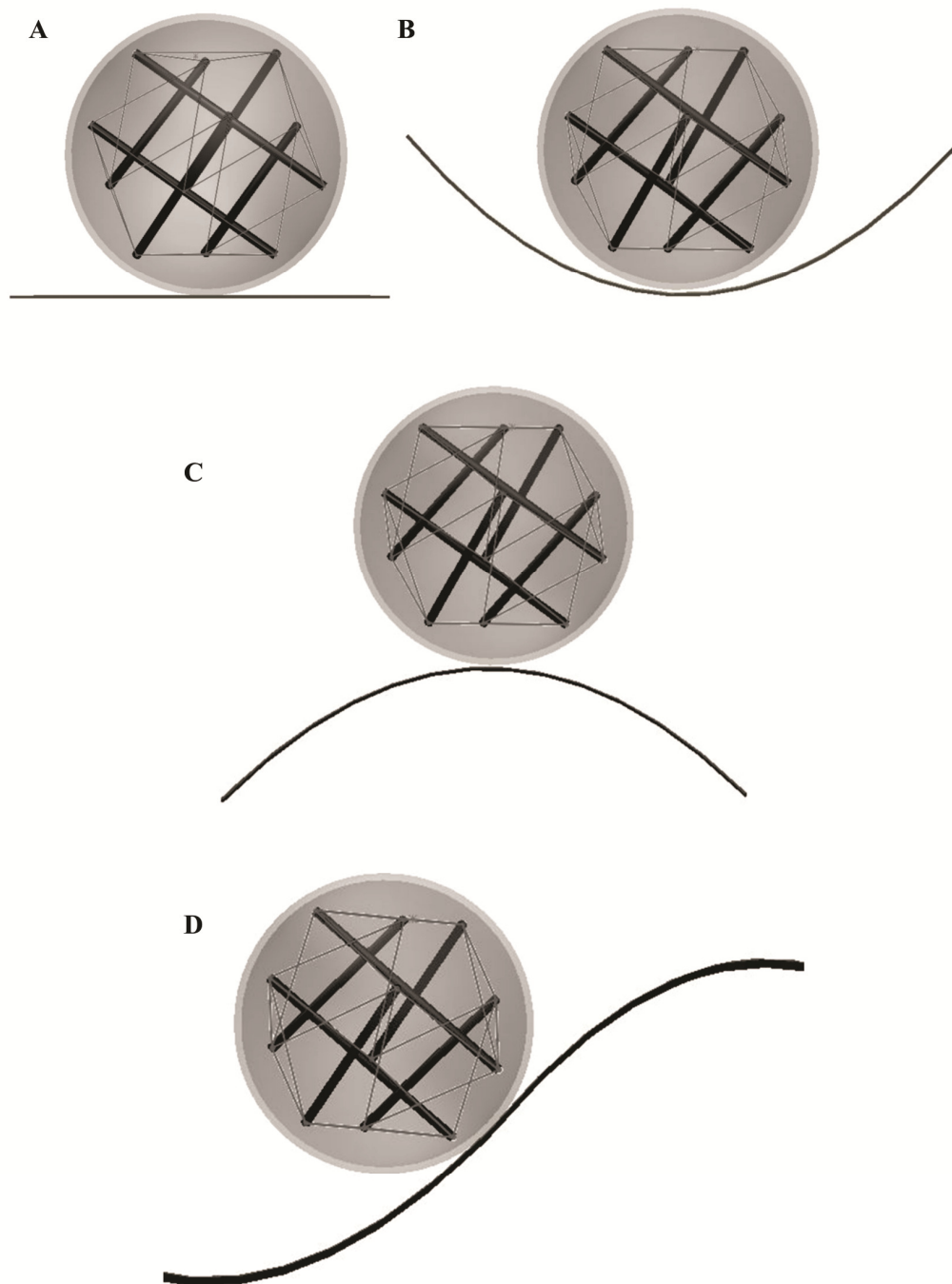
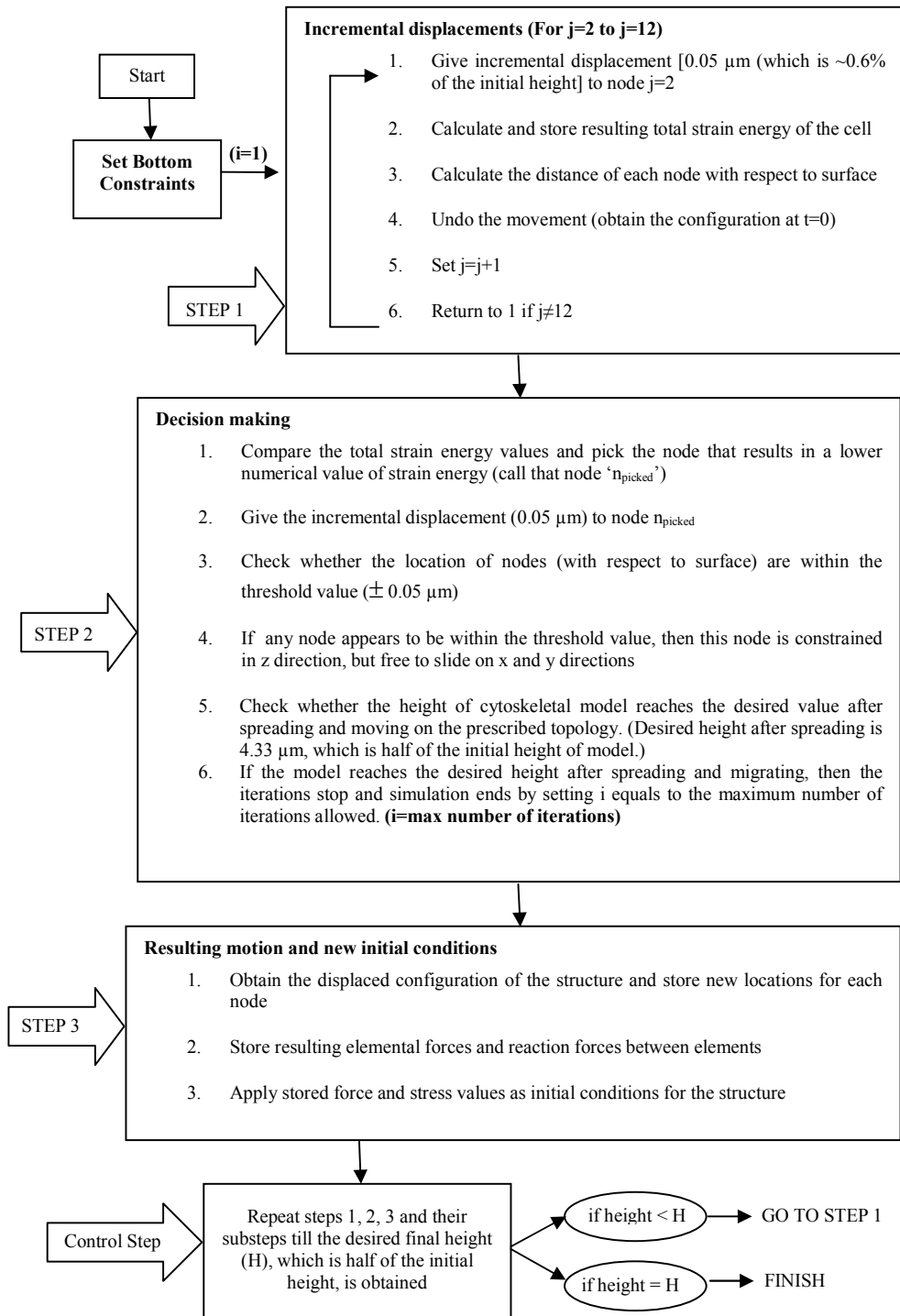**Figure 3**: Initial configurations of the cell model located on the flat surface (A); trough (B), peak (C) and slope (D) positions of the wavy surface

Incremental displacements (For j=2 to j=12)

1. Give incremental displacement [0.05 μm (which is ~0.6% of the initial height] to node j=2

2. Calculate and store resulting total strain energy of the cell

3. Calculate the distance of each node with respect to surface

4. Undo the movement (obtain the configuration at t=0)

5. Set j=j+1

6. Return to 1 if j≠12

Start

Set Bottom Constraints **(i=1)**

STEP 1

Decision making

1. Compare the total strain energy values and pick the node that results in a lower numerical value of strain energy (call that node 'n_{picked}')

2. Give the incremental displacement (0.05 μm) to node n_{picked}

3. Check whether the location of nodes (with respect to surface) are within the threshold value ($\pm$ 0.05 μm)

4. If any node appears to be within the threshold value, then this node is constrained in z direction, but free to slide on x and y directions

5. Check whether the height of cytoskeletal model reaches the desired value after spreading and moving on the prescribed topology. (Desired height after spreading is 4.33 μm, which is half of the initial height of model.)

6. If the model reaches the desired height after spreading and migrating, then the iterations stop and simulation ends by setting i equals to the maximum number of iterations allowed. **(i=max number of iterations)**

STEP 2

Resulting motion and new initial conditions

1. Obtain the displaced configuration of the structure and store new locations for each node

2. Store resulting elemental forces and reaction forces between elements

3. Apply stored force and stress values as initial conditions for the structure

STEP 3

Control Step

Repeat steps 1, 2, 3 and their substeps till the desired final height (H), which is half of the initial height, is obtained

if height < H → GO TO STEP 1

if height = H → FINISH

Figure 4: Flow chart of the simulation process

Figure 5: Final spread configurations of the cytoskeletal model at the end of simulations on flat surface (A), and trough (B), peak (C) and slope (D) positions of the wavy surface for non-rotated case initial constraint set 2. XZ – is the cross section of the wavy plate and XY – is the top view of the plate
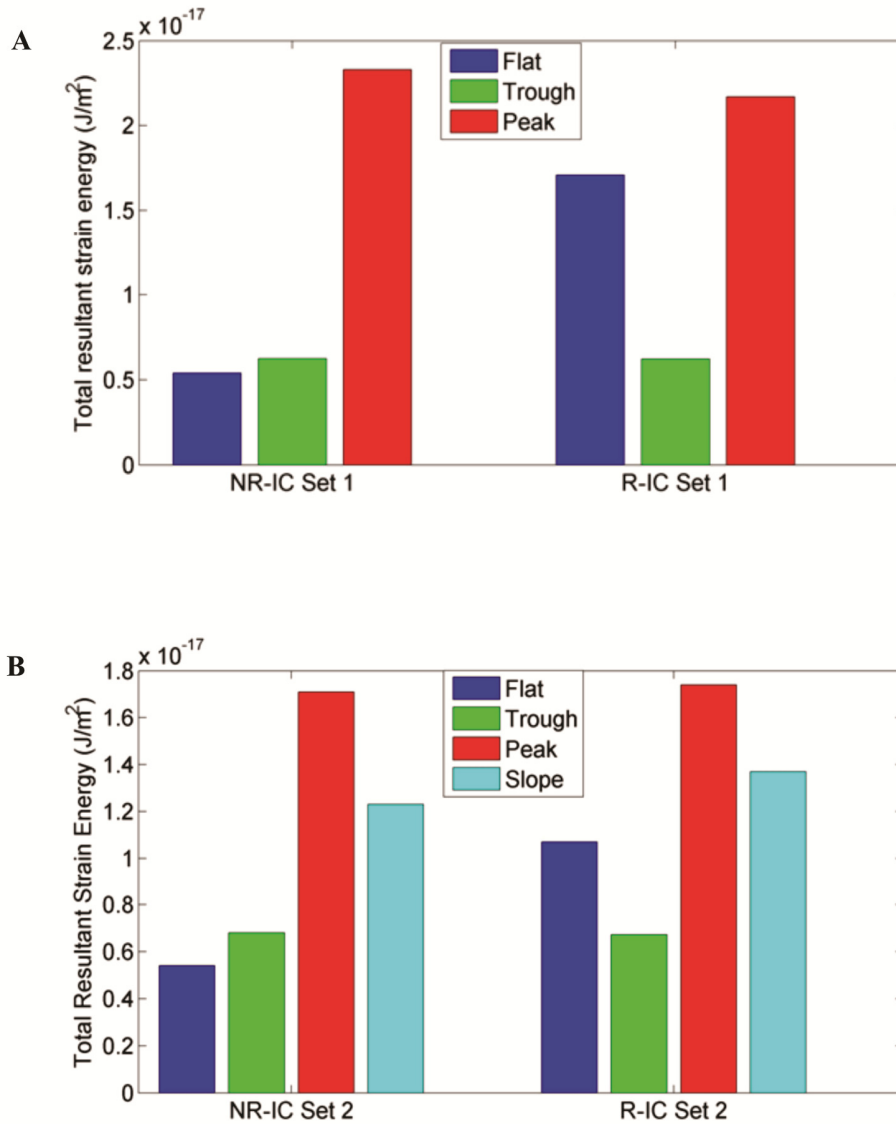
41

Figure 6: The resultant strain energy values for the final spread configurations of the cell on different surface topologies for the initial constraint set 1 (IC Set 1) case (A); for the initial constraint set 2 (IC Set 2) case (B). Simulations obtained by placing the cell initially on the slope position are only executed by anchoring one node to the surface (IC Set 2) due to the cell's initial position with respect to surface. Thus, IC Set1 is not applied to the slope position cases. (NR=non-rotated model, R=rotated model)

Figure 7: Total number of iterations within the simulation process until the cell model becomes spread on prescribed surfaces (the cell reaches half of its initial height). IC Set1 is not applied to the slope position cases. (NR=non-rotated model, R=rotated model)

Figure 8: Alignment angle definition

Figure 9: Alignment angle definition on ellipsoid

Figure 10: Ellipsoids fitted to coordinate data for the final spread configurations of the model that are initially placed at flat (A), trough (B), and peak (C) positions of wavy surface (NR-IC Set 1 case)

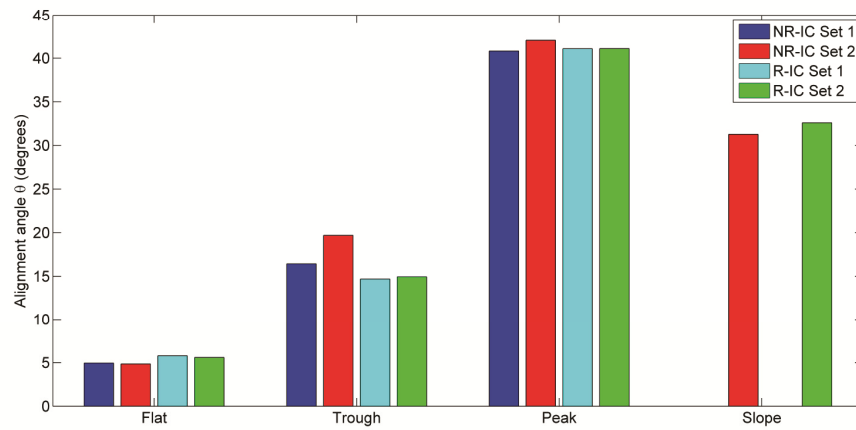**Figure 11:** Ellipsoids fitted to coordinate data for the final spread configurations of the model that are initially placed at flat (A), trough (B), slope (C), and peak (D) positions of wavy surface (NR-IC Set 2 case)

Figure 12: Ellipsoids fitted to coordinate data for the final spread configurations of the model that are initially placed at flat (A), trough (B), and peak (C) positions of wavy surface (R-IC Set 1 case)

Figure 13: Ellipsoids fitted to coordinate data for the final spread configurations of the model that are initially placed at flat (A), trough (B), slope (C), and peak (D) positions of wavy surface (R-IC Set 2 case)

Figure 14: Alignment angles for different set of initial conditions and orientations for the model initially located at flat, trough, slope, and peak positions of the wavy surface (NR=non-rotated, R=rotated)

Figure 15: Scatter plot of the centroids, where red point represents the centroid of the undeformed (initial) model: isometric view (A), top view (XY plane) (B), and front view (XZ plane) (C) (F = flat, T=trough, P = peak, S = slope)

50

Figure 16: Spreading areas on the prescribed surface profiles for the final spread configurations of the model (NR=non-rotated, R=rotated)
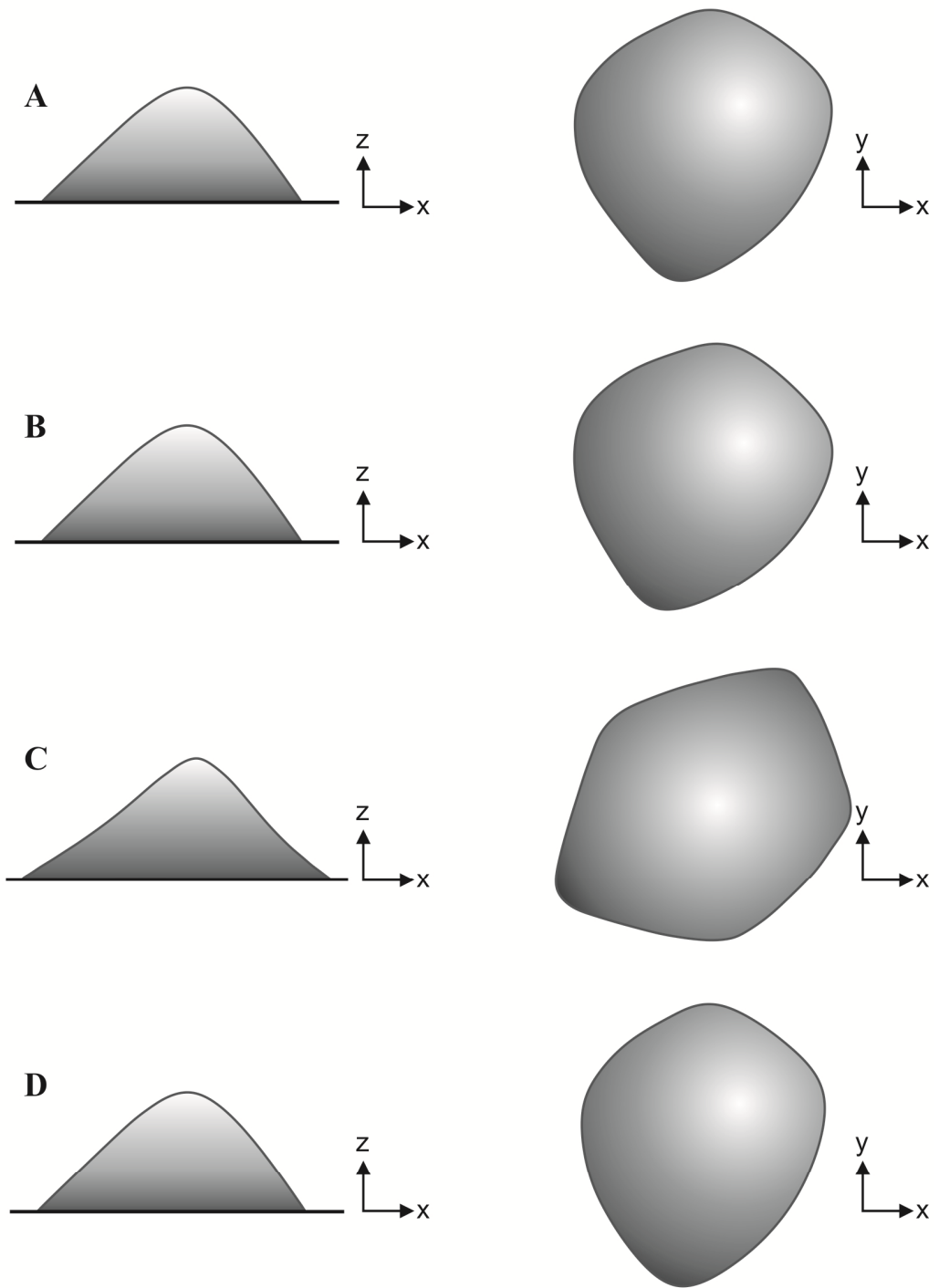
Figure A1: Final spread configurations of the cytoskeletal model at the end of simulations on flat surface for non-rotated case initial constraint set 1 (A) and initial constraint set 2 (B), for rotated case initial constraint set 1 (C) and initial constraint set 2 (D). XZ – is the cross section of the wavy plate and XY – is the top view of the plate
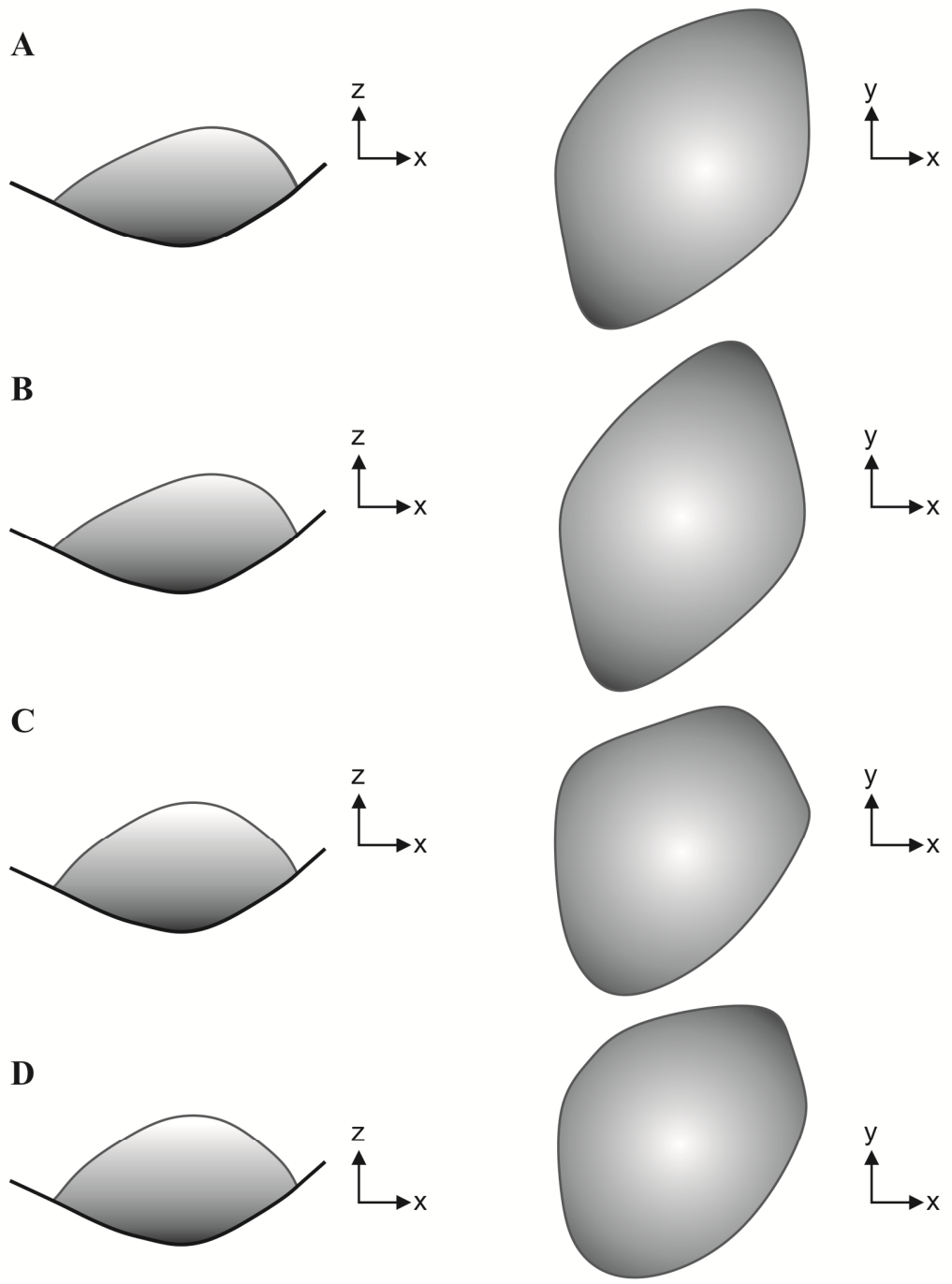
Figure A2: Final spread configurations of the cytoskeletal model at the end of simulations on trough position of wavy surface for non-rotated case initial constraint set 1 (A) and initial constraint set 2 (B), for rotated case initial constraint set 1 (C) and initial constraint set 2 (D). XZ – is the cross section of the wavy plate and XY – is the top view of the plate
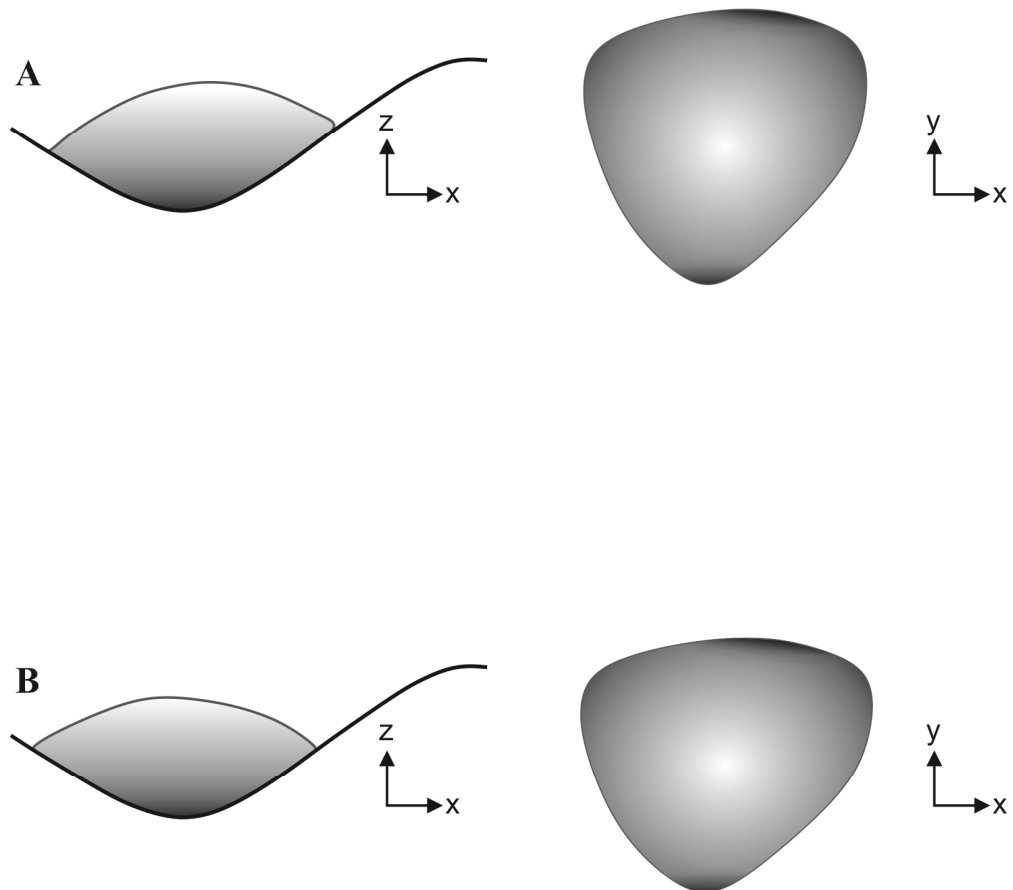
Figure A3: Final spread configurations of the cytoskeletal model at the end of simulations on slope position of wavy surface for non-rotated case initial constraint set 2 (A) and rotated case initial constraint set 2 (B). XZ – is the cross section of the wavy plate and XY – is the top view of the plate
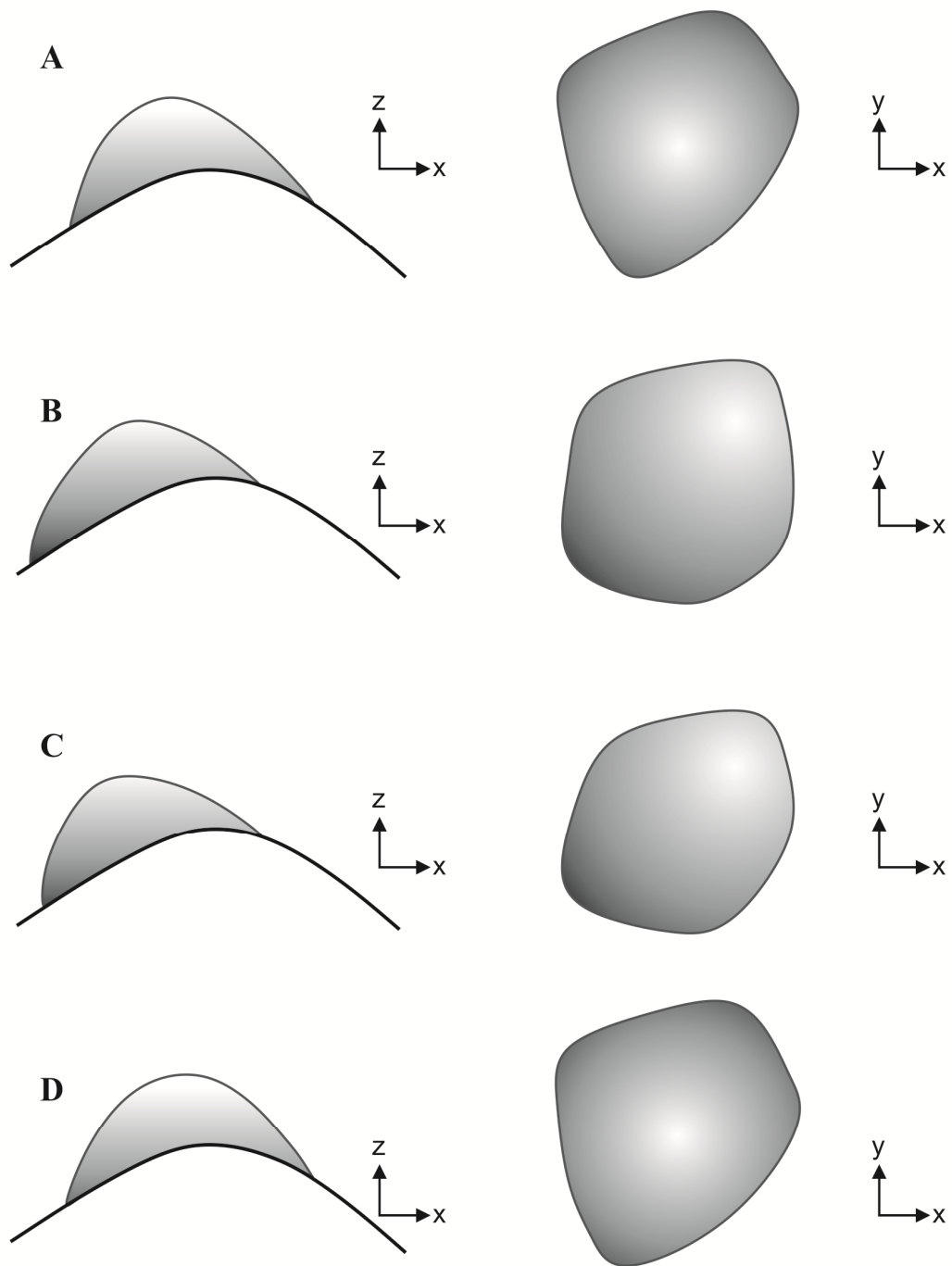
Figure A4: Final spread configurations of the cytoskeletal model at the end of simulations on peak position of wavy surface for non-rotated case initial constraint set 1 (A) and initial constraint set 2 (B), for rotated case initial constraint set 1 (C) and initial constraint set 2 (D). XZ – is the cross section of the wavy plate and XY – is the top view of the plate

VITA

Ezgi Pinar Yalcintas was born in Istanbul, Turkey on March 31, 1990 as the daughter of Gunseli and Huseyin Yalcintas. She received a Bachelor of Science degree in Mechanical Engineering from Middle East Technical University, in June of 2012, then joined the Master of Science graduate program of the Department of Mechanical Engineering and Mechanics at Lehigh University in Bethlehem, Pennsylvania. She was advised for this Master's thesis by Arkady Voloshin.